A phase transition creates the geometry of the continuum from discrete space

Robert S. Farr[a,b,1] **and Thomas M.A. Fink**[b]

[a]Jacobs Douwe Egberts, Banbury, Oxfordshire, UK; [b]London Institute for Mathematical Sciences, Mayfair, London, UK

This manuscript was compiled on April 11, 2019

Models of discrete space and space-time that exhibit continuum-like behavior at large lengths could have profound implications for physics. They may tame the infinities that arise from quantizing gravity, and dispense with the machinery of the real numbers, which has no direct observational support. Yet despite sophisticated attempts at formulating discrete space, researchers have failed to construct even the simplest geometries. We investigate graphs as the most elementary discrete models of two-dimensional space. We show that if space is discrete, it must be disordered, by proving that all planar lattice graphs exhibit the same taxicab metric as square grids. We give an explicit recipe for growing disordered discrete space by sampling a Boltzmann distribution of graphs at low temperature. We then propose three conditions which any discrete model of Euclidean space must meet: have a Hausdorff dimension of two, support unique straight lines and obey Pythagoras' theorem. Our model satisfies all three, making it the first discrete model in which continuum-like behavior is recovered at large lengths.

Networks | Graphs | Emergent space | Geometry | Phase transitions

The small-scale structure of space has puzzled scientists and philosophers throughout history. Zeno of Elea (1) claimed that geometry itself is impossible because there is no consistent form this small-scale structure can take. He argued that a line segment, which can be halved repeatedly, cannot ultimately be composed of pieces of non-zero length, else it would be infinitely long. However, it also cannot be composed of pieces of zero length, for no matter how many are added together, the resulting line will never be longer than zero.

It is a lasting tribute to the optimism of researchers that work on geometry nevertheless carried on. Soberingly, it was not until the 19$^{\text{th}}$ century – nearly two and a half millennia later – that Cantor finally resolved the paradox by defining the continuum. He showed that the line must be composed not just of an infinite number of points, but of an *uncountably* infinite number, so that the second half of Zeno's argument fails. This uncountable infinity is described by the mathematical machinery of the real numbers. The continuum is the basis for all descriptions of space and space-time, and therefore all of theoretical physics.

In the 20$^{\text{th}}$ century, Weyl (2) further claimed that the continuum is the only possible model of space. He constructed a tiling argument, purporting to show that if space is discrete, Pythagoras' theorem – or, equivalently, the Euclidean metric – is false. Weyl's proof, however, contains an unstated assumption which turns out to be the key to its resolution.

Despite this long belief in the necessity of the continuum, researchers are actively pursuing discrete (3–5), or at least piece-wise flat (6–10), models of space and space-time, as they offer the possibility to remove non-renormalizable infinities which arise in simple versions of quantum gravity. All these models can be thought of as graphs, where just the graph itself matters, not its embedding into another space. The only natural metric in this case is graph geodesic distance: the distance between two nodes is the smallest number of edges joining them.

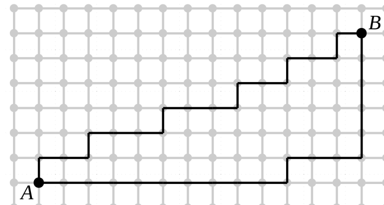

Fig. 1. The geometry of the square grid graph. Two nodes A and B on the square grid graph are separated by 19 edges. There are many possible shortest paths (geodesics) of length 19 edges between the nodes, of which two are shown in black. The resemblance to the possible routes followed by yellow cabs in New York city inspired the term 'taxicab metric' for the measure of distance on this graph (14).

In two dimensions, toy models of 'quantum graphity' aim to produce planar graphs made up of triangles but, so far (11, 12), with little success. A final problem encountered with graph models is that completely random triangulations of the plane do not even have dimension two. They are so crumpled that the number of nodes in a disc of radius r scales as r^4, not r^2 (13).

In light of these difficulties, the prospects for building a consistent discrete model of even the Euclidean plane seem poor. In this Article, we show that it is in fact possible to discretize space. We do three things. First, we prove

Significance Statement

Is space a continuum or is it composed of a discrete set of points? Once a purely philosophical question, there is now a pressing need to describe space and space-time as discretized, in order to tame the infinities that arise from quantizing gravity. However, attempts to create a model of points and edges – a graph – which satisfies Euclid's postulates at large lengths, have so far been unsuccessful. We prove that if space is discrete, it must be disordered. We then provide an explicit recipe for growing disordered graphs that satisfy Euclidean geometry. Our work is an important step in the search for discrete models of space.

Author contributions: R.S.F. conceived the study, and designed and performed the computer simulations. R.S.F. and T.M.A.F. contributed equally to the mathematical proofs and to writing the manuscript.

The authors declare no conflict of interest

[1]To whom correspondence should be addressed. E-mail: robert.farr@JDEcoffee.com

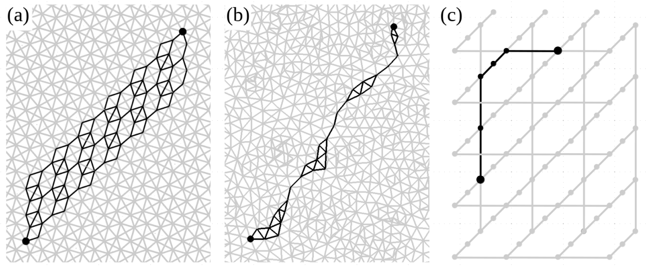

Fig. 2. Geodesic confinement is not found in planar lattice graphs but is in planar disordered graphs. (a) In a doubly-periodic triangulation (a modified snub square tiling), two nodes marked as circles are 22 edges apart. We call the set of all geodesics between them (shown in black) the geodesic bundle, containing a number of nodes proportional to the square of the geodesic length. (b) In a random triangulation, the geodesic bundle between two nodes 22 edges apart is confined to a narrow region. We call this phenomenon geodesic confinement. (c) A nonplanar doubly periodic graph (all nodes shown as circles) has neither a taxicab nor Euclidean metric.

that any discrete model of two-dimensional space must be disordered, by showing that all planar lattice graphs have a taxicab metric (14). Order is the hidden assumption in Weyl's proof of the impossibility of discrete space. Second, we describe a local, statistical process, with an associated temperature, which provides an explicit recipe for growing disordered graphs. Third, we propose three tests which any model of Euclidean space must pass. We find that graphs grown by our thermal process, at low temperature, achieve the required properties: they have a Hausdorff dimension of 2, support the existence of unique straight lines, and satisfy Pythagoras' theorem.

1. Lattice graphs are taxicab graphs

The natural way to measure the distance between two nodes on a graph is to count the edges in the shortest path which separates them. A shortest path of this kind is called a geodesic. It is well known that with this measure of distance, the square grid graph has a taxicab geometry (14), where the distance between two nodes is the sum of the magnitude of the differences of their Cartesian coordinates (Figure 1). There are typically many geodesics between two nodes a distance λ apart, each resembling an irregular staircase. Together these form a geodesic bundle comprising $N_{\mathrm{geo}} \propto \lambda^2$ nodes. More complex lattice graphs show a similar phenomenon (Figure 2a).

We prove that all doubly-periodic planar graphs have the taxicab metric, regardless of the complexity of the unit cell. Such graphs therefore do not satisfy Euclid's axiom of a unique straight line between two points, nor Pythagoras' theorem. Our proof is in two parts, which we call geodesic composition and geodesic rearrangement. We sketch the proof here, and give full details in the Methods section.

Sketch of the proof. If we have a geodesic on a graph, it is clear that cutting it in two yields two paths which are also geodesics. Even in classical geometry, however, putting two geodesics (straight lines) end-to-end does not always give a geodesic: they need to be parallel. The situation with graphs is more interesting still.

A doubly periodic planar graph must belong to one of the wallpaper groups, familiar from crystallography (and interior design). It will have a unit cell that may contain more than one node. Equivalent nodes in different unit cells are said to be of the same type. We first construct a geodesic between two nodes of the same type, which are separated by a vector distance (m, n) unit cells. If we choose the node type so that this is the shortest of all such geodesics (or one of the shortest, if the choice is not unique), then we are able to prove that many copies of this path can be concatenated end-to-end, and the result is still a geodesic. We call this the geodesic composition property, and it is not trivial, since it can fail for non-planar doubly-periodic graphs (Figure 2c).

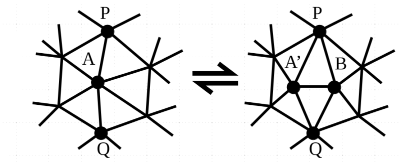

Fig. 3. Steinitz moves on a portion of a triangulation. The push move (left to right) consists of choosing a node A and two (nearly, if Z is odd) opposite neighbors P and Q. Node A is divided into nodes A' and B. The pop move (right to left) consists of choosing a node A', and then one of its neighbors B. If no neighbor of A' that is not P, Q or B is connected to a neighbor of B that is not P, Q or A', then A' and B are merged into A. In contrast to (17), which keeps track of triangular faces, we avoid tetrahedra and bottlenecks smaller than 4 edges, so faces can be assigned unambiguously, if desired.

Next, we show that a long concatenation of this single type of geodesic can, apart from short tails at the ends, be broken down into many alternating copies of two different geodesics. The proof uses Dedekind's pigeonhole principle (15), applied to the number of nodes in the unit cell. If m and n are relatively prime, these two geodesics are not parallel. They therefore perform the role of the coordinate directions in the square grid graph, and in the same way, can be re-arranged in any order to produce many irregular staircase-like geodesics, all of the same length. The set of these geodesics forms the broad geodesic bundle, with an area proportional to the square of its length: a complete contrast to the narrow lines required by Euclidean geometry.

2. Growing disordered graphs

In light of the impossibility of generating Euclidean geometry from planar lattice graphs, we turn to disordered graphs which triangulate the 2-sphere. Triangulations here are graphs composed of triangles which, when embedded in the 2-sphere, are planar (16). We also require that they contain no tetrahedra. We start from a seed graph, the octahedron, which is a simple triangulation of the 2-sphere. We grow this through a series of local Steinitz moves (17), which add ('push') or remove ('pop') nodes while preserving this property (Figure 3). After growth to a size of N nodes with push moves, we apply $8N$ alternating push and pop moves to ensure equilibration.

All triangulations of the 2-sphere can can be transformed into one another by Steinitz moves (17). Because every triangular face has three edges, and every edge belongs to two triangles, Euler's polyhedron theorem (18) implies that the mean degree of all nodes in a triangulation is

$$\langle Z \rangle = 6 - 12/N. \qquad [1]$$

Since the integrated Gaussian curvature over a smooth, closed surface is 4π (19), we see that if Z is the degree of a node, $\kappa \equiv 6 - Z$ is a natural measure of the local, discrete

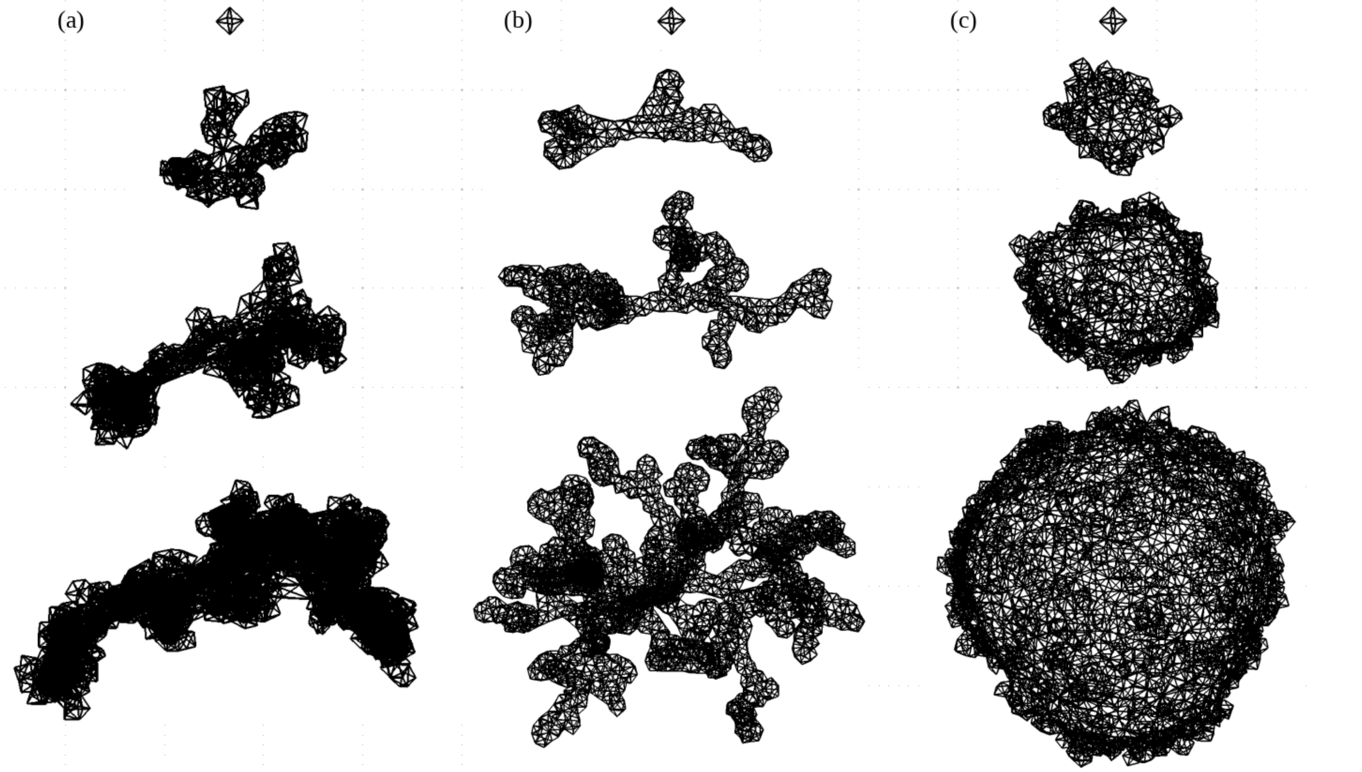

Fig. 4. Growing graphs at hgh and low temperatures; the third column shows the main result of this Article: a discrete model of Euclidean space. A small octahedral triangulation, with $N = 6$ can be grown and equilibrated into larger graphs with $N = 2^8$, 2^{10} and 2^{12} nodes at (a) high temperature, (b) $T = 0.5$ in the curvature model, or (c) low temperature in the walker model. The illustrative embedding into space shown here is irrelevant to our results; we are only interested in the graph.

equivalent of Gaussian curvature for the triangulation, up to a constant factor. If we consider a patch of the graph consisting of N_{pat} nodes, with e exiting edges, and with a simple closed-path perimeter of length $p \geq 3$ edges, then the Euler characteristic implies the average discrete curvature over all nodes in the patch is

$$\langle\kappa\rangle_{\mathrm{pat}} = (6 + 2p - e)/N_{\mathrm{pat}}. \qquad [2]$$

Thus a Steinitz push move locally decreases $|\langle\kappa\rangle_{\mathrm{pat}}|$, and a pop move increases it.

To create an ensemble of graphs, we first define an energy E for every graph. We then repeatedly select a random node as a candidate for a push or pop move, and calculate the energy change ΔE that would result. We perform the move with a probability given by the Metropolis algorithm (20) with an associated temperature T.

Curvature model. The most obvious choice of energy to reduce curvature fluctuations at low temperature is $E_{\mathrm{curv}} = \sum_i \kappa_i^2$, where the sum is over all nodes i. As shown in Figure 4 and also considered in (21), this does indeed drive the local curvature to zero almost everywhere at low temperature, but it does so by creating a branched polymer phase consisting of thin tubes with curvature trapped at their ends and junctions (Figure 4b). The result of this 'curvature model' is far from flat. We attribute this to the energy functional failing to sufficiently penalize small curvatures spread over large areas.

Walker model. To address the deficiency of the curvature model, we introduce a second statistical process by putting walkers on the graph. Walker models have previously been used to create scale-free (22) graphs from local rules (23, 24), but here we are interested in Euclidean behavior. At each time step, we add κ walkers of type $+1$ to every node with $\kappa > 0$, and $|\kappa|$ walkers of type -1 to every node with $\kappa < 0$. Additionally, 12 walkers of type -1 are added to random nodes to maintain the mean walker number from eq. (1). The walkers then diffuse by moving to a random neighboring node. Whenever a $+1$ and a -1 walker occupy the same node, both walkers annihilate. Walker moves alternate with push-pop moves, and we replace E_{curv} with a new energy E_{walk} for the graph under push-pop moves:

$$E_{\mathrm{walk}} = -\sum_i w_i|w_i|, \qquad [3]$$

where w_i is the net number of walkers on node i. At low temperatures, this energy tends to shrink regions of positive curvature and grow regions of negative curvature. We call this new evolution scheme, which biases the graph towards flatness on long length scales, the 'walker model'.

The walker model generates a triangulation which, at low temperature and long lengths, appears qualitatively to have minimal curvature (Figure 4c). To establish that these graphs satisfy Euclidean geometry at long length scales, we subject them to three tests: a Hausdorff dimension of 2; geodesic confinement; and the Pythagorean theorem.

3. Testing our graphs

Euclidean geometry is defined through five axioms. These are neither as logically primitive as they first appear, nor do they

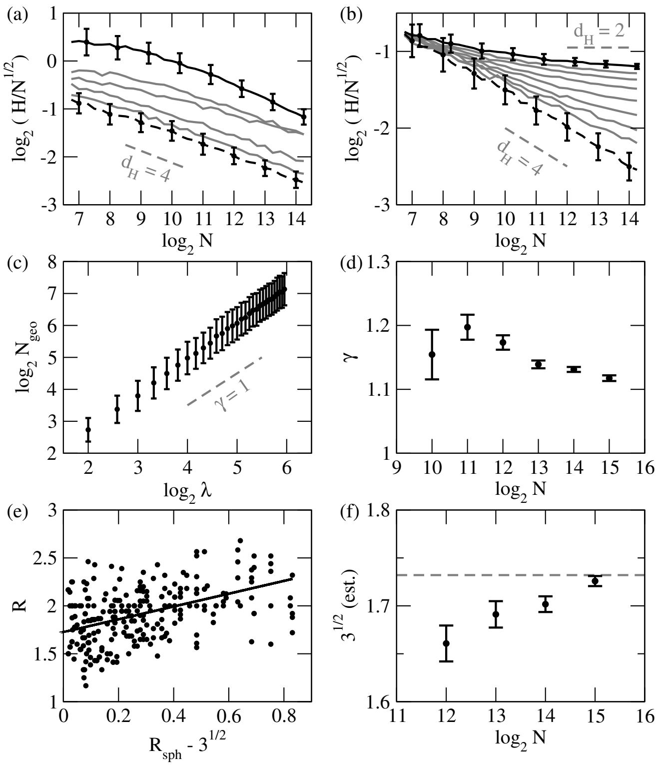

Fig. 5. Statistical tests for Euclidean behavior of our grophs. Top row: The mean node eccentricity H and standard deviation for example points, divided by $N^{1/2}$, where N is the number of nodes. (a) The curvature model with $T = 0.5$ (black), 2^0, 2^2, 2^4, 2^6 (gray) and 10^5 (dashed) (b) The walker model, with $T = 2^{-3}$ (black), 2^2, 2^3, $2^4 \ldots 2^8$ (gray) and 10^5 (dashed). Middle row: (c) The number of nodes $N_{\rm geo}$ in geodesic bundles of different lengths λ on a low-temperature walker model graph with $N = 2^{15}$ nodes. (d) Fitted values for γ, where $N_{\rm geo} \propto N^\gamma$ for graphs of different N. Bottom row: R is the ratio of the perpendicular length to the edge side of an equilateral triangle drawn on a low-temperature walker model with $N = 2^{15}$ nodes. $R_{\rm sph}$ is the exact equivalent on a smooth sphere [eq. (5)]. (e) R plotted against $R_{\rm sph} - \sqrt{3}$ (we show a random sample of 250 from the full set of 6078 points). The line is a linear regression and we extract the intercept as a graph-theoretic estimate of $\sqrt{3}$. (f) Estimates of $\sqrt{3}$ by this method for graphs of different size N. The dashed gray horizontal line is the exact value.

readily translate into conditions for discrete models of space. We therefore propose three conditions for any discrete model, including ours, purporting to capture Euclid's geometry at large lengths. The first, Hausdorff dimension, sits outside the original axioms, since they concerned the plane. The second condition is the appearance of straight lines in the large length limit, which we call geodesic confinement. The third is the Euclidean metric itself, commonly known as Pythagoras' theorem, which is a synthesis of all the axioms.

Hausdorff dimension. If the number of nodes in a ball of radius r scales as $N \propto r^{d_H}$, then d_H is the Hausdorff dimension of the graph. Interestingly, it is known that random triangulations of the 2-sphere lead to graphs with $d_H = 4$ as they converge to 'Brownian maps' (13). To calculate the dimension of our graphs, we define the half-circumference H of a graph as the average over all nodes of the node eccentricity, where the eccentricity of a node is the greatest geodesic distance between it and any other node in the graph. If nodes are a measure of area, then we would expect a graph which approximates a smooth spherical surface with $d_H = 2$ to satisfy the scaling $H \propto N^{1/2}$. This is not the case for the curvature model (Figure 5a), but is true for the walker model in the low temperature limit for a large number of nodes (Figure 5b). The upwards curvature of the solid gray lines in Figure 5b shows evidence that this phase persists at non-zero temperature.

Geodesic confinement. In a doubly-periodic graph, the total number of nodes $N_{\rm geo}$ in the geodesics between two nodes a distance λ apart scales as $N_{\rm geo} \propto \lambda^2$. From Figure 5cd, we see that the scaling of $N_{\rm geo}$ with N also approximates a power law for the low-temperature walker model, but with a different exponent:

$$N_{\rm geo} \propto N^\gamma \quad \text{with} \quad \gamma \approx 1.1. \qquad [4]$$

An exponent $\gamma < 2$ implies qualitatively different behavior to the doubly-periodic lattice case, and in the limit $N \to \infty$, it is consistent with the narrow geodesics ('straight lines') familiar from Euclidean geometry. We call the collapse of the broad, $N_{\rm geo} \propto \lambda^2$ geodesic bundles 'geodesic confinement' (Figure 2b), in analogy to the flux tubes and color confinement seen in strong-force interactions (25).

Pythagorean theorem. Finally we consider the validity of Pythagoras' theorem on graphs generated by the walker model. Although this can be proved in general for Euclidean geometry, on graphs we are only able to provide a test. If we draw an equilateral spherical triangle on a smooth 2-sphere, with side-length Λ times the half-circumference, the ratio of the length of the perpendicular of the triangle to half its edge length is found, from spherical trigonometry, to be

$$R_{\rm sph}(\Lambda) \equiv \frac{2}{\pi\Lambda} \arccos\left[\frac{\cos(\pi\Lambda)}{\cos(\pi\Lambda/2)}\right] = \sqrt{3} + O(\Lambda^2). \qquad [5]$$

The same ratio R can be calculated for a graph (Figures 5ef, 6), and although the fluctuations are significant, they appear to be unbiased, so that performing linear regression of R against $R_{\rm sph}$ gives an estimate for $\sqrt{3}$ one standard deviation from the traditional value:

$$\sqrt{3}_{\rm est} = 1.726 \pm 0.005. \qquad [6]$$

4. Methods

Our proof that all planar lattice graphs satisfy the taxicab metric is in two parts, which we call geodesic composition and geodesic rearrangement:

Geodesic composition. Consider a doubly-periodic planar graph made up of identical unit cells, each of which comprises ω distinct nodes. Equivalent nodes in different unit cells are said to be of the same type. Let $\mathcal{G}_{pp}(\mathbf{v})$ denote a particular geodesic between two p-type nodes separated by $\mathbf{v} = (m, n)$ unit cells.

We first prove that for any displacement $\mathbf{v}$, for at least one node type p, the concatenation $\mathcal{G}_{pp}(k\mathbf{v})$ of k copies of $\mathcal{G}_{pp}(\mathbf{v})$ is also a geodesic (Figure 7a–d). Let p be the node type which minimizes $\mathcal{G}_{pp}(\mathbf{v})$; call this the optimal node assumption. Let p_0p_1 of length $|p_0p_1| = \lambda$ be a geodesic between p_0 and p_1 (Figure 7a); call this the $\mathbf{v}$-geodesic assumption. Let $p_0p_1p_2$ be two copies of p_0p_1.

Now suppose there is a path p_0abp_2 with length $|p_0abp_2| < |p_0p_1p_2| = 2\lambda$ (Figure 7b); because the graph is planar, nodes a and b exist. Then $|ab| < \lambda$ or $|p_0a| + |bp_2| < \lambda$. If the former,

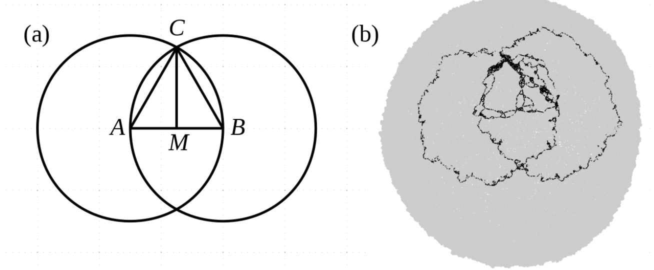

Fig. 6. Equilateral triangles on the plane and on a graph. (a) An equilateral triangle drawn on the Euclidean plane with straightedge and compass, where M is half-way between A and B, and $MC/AM = \sqrt{3}$. (b) The same construction using geodesics on a low-temperature 'walker model' graph (which approximates a smooth sphere) with $N = 2^{16}$ nodes and triangle side length of 32.

then we contradict the optimal node assumption. If the latter, we contradict the $\mathbf{v}$-geodesic assumption. Therefore $p_0p_1p_2$ is a geodesic between p_0 and p_2. That is to say, $\mathcal{G}_{pp}(2\mathbf{v})$, which is the concatenation of 2 copies of $\mathcal{G}_{pp}(\mathbf{v})$, is a geodesic. Call this the $2\mathbf{v}$-geodesic property.

We now show that the $(k-1)\mathbf{v}$-geodesic property implies the $k\mathbf{v}$-geodesic property (Figure 7c for $k = 3$). Suppose there is a path p_0abp_k with length $|p_0abp_k| < |p_0p_1 \ldots p_k| = k\lambda$. Then $|ab| < \lambda$ or $|p_0a| + |bp_k| < (k-1)\lambda$ (Figure 7d for $k = 3$). If the former, then we contradict the optimal node assumption. If the latter, then we contradict the $(k-1)\mathbf{v}$-geodesic property. Therefore $p_0p_1 \ldots p_k$ is a geodesic between p_0 and p_k. This completes the first part of the proof.

Geodesic rearrangement. We next prove that for most displacements $\mathbf{v}$, for at least one node type p, the geodesic $\mathcal{G}_{pp}(k\mathbf{v})$ consists of three parts: a tail at each end, which joins the nodes p_0 and p_k to copies of some other type of node q, and between the tails, $k-1$ alternating copies of $\mathcal{G}_{qq}(\mathbf{u})$ and $\mathcal{G}_{qq}(\mathbf{u}')$ (Figure 7ef). We now only consider displacement vectors $\mathbf{v} = (m, n)$ such that m and n are relatively prime (which occurs (26) for random m and n with probability $6/\pi^2 \simeq 0.61$) and large enough so that $\lambda > 2\omega$, where ω is the number of distinct nodes in the unit cell. By Dedekind's pigeonhole principle (15), since $\lambda/\omega > 2$, $\mathcal{G}_{pp}(\mathbf{v})$ must pass through at least two nodes of some other type q different from type p (Figure 7e). Therefore we can define a sub-geodesic $\mathcal{G}_{qq}(\mathbf{u})$ within $\mathcal{G}_{pp}(\mathbf{v})$, and a second geodesic $\mathcal{G}_{qq}(\mathbf{u}')$ between the node q in adjacent copies of $\mathcal{G}_{pp}(\mathbf{v})$ (Figure 7f).

Because m and n are relatively prime, $\mathbf{u}$ and $\mathbf{u}'$ cannot be parallel. To see why, let the displacement $\mathbf{u}$ be (i, j) and the displacement $\mathbf{u}'$ be (i', j') and assume $i' \geq i$. Since $\mathbf{u} \parallel \mathbf{u}'$ implies $i/j = i'/j'$, $(m, n) = (i + i', j + j') = (1 + i'/i)(i, j)$, where i'/i is an integer, contradicting (m, n) being relatively prime.

The $k-1$ alternating geodesics can be rearranged in any order, forming a set of staircases between the end q nodes (Figure 7f). The geodesic bundle occupies an area of $mn(k-1)^2$ unit cells. This completes the proof.

Computer code. The simulation code to generate the figures and statistics is available from from Sourceforge under the name 'ThermalEuclid'. The code is written in the C programming language, using the open source 'freeglut' library for graphics.

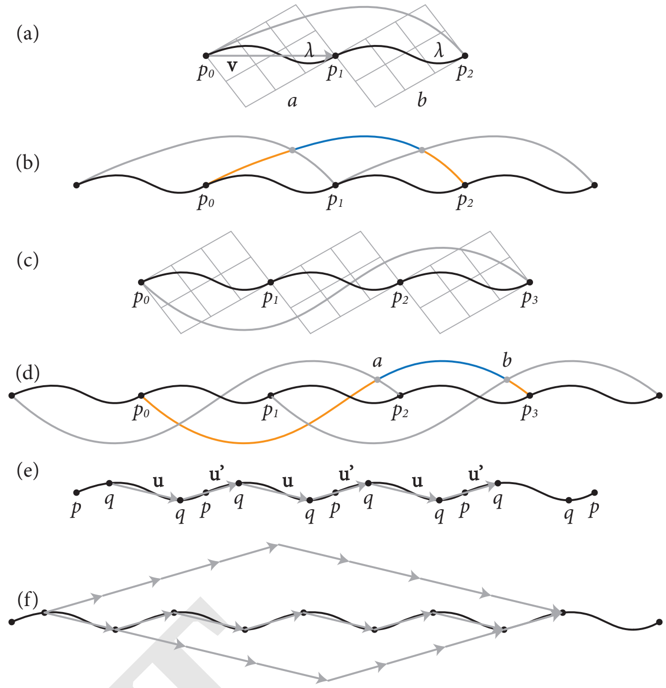

Fig. 7. All doubly-periodic planar graphs have a taxicab metric on long length scales. (abcd) A grid of unit cells forms a doubly-periodic planar graph; nodes within the unit cells not shown. For some node type p, if p_0p_1 is a shortest path between nodes separated by $\mathbf{v} = (m, n)$ unit cells, then $p_0p_1 \ldots p_k$ is the shortest path between nodes separated by $k\mathbf{v}$ unit cells. (ef) For m and n relatively prime, the geodesic $\mathcal{G}_{pp}(k\mathbf{v})$ is the concatenation of $k-1$ copies of both $\mathcal{G}_{qq}(\mathbf{u})$ and $\mathcal{G}_{qq}(\mathbf{u}')$, with tails at either end. See the text for details.

5. Discussion

We have shown that discrete space and Euclidean space, thought by many to be at odds, are indeed compatible. We avoid Zeno's paradox because we do not require our model to be infinitely divisible. We avoid Weyl's tiling argument because our model is disordered. Weyl's argument is in fact an observation that certain non-planar lattices display the taxicab metric, which is unsurprising given our proof that all planar lattice graphs do.

No embedding space. Smooth surfaces which are discrete at an atomic scale frequently arise in nature, such as liquid menisci or crystal surfaces (27). These atomic systems are embedded in a background manifold, consisting of ordinary, flat, three-dimensional space. This embedding manifold allows distance on the surface to be defined in the usual Euclidean manner, and also means that normals to the surface exist. The system energy can then depend on extrinsic curvature (the spatial gradient of these normals), as well as intrinsic (Gaussian) curvature. Our graphs, by contrast, do not live in a background space. Instead, our measure of distance and curvature can only be intrinsic, defined in terms of edges (distance) and node degree (curvature) that are properties of the graph itself. No normal vectors to our graph manifolds exist.

Phase transition. Phase transitions which create or destroy smoothness are well known in physics. A roughening transition (27) can turn flat crystal facets into smooth, curved surfaces, as measured with the metric of the embedding space.

More strikingly, the crumpling transition of membranes (28) turns flat crystalline membranes into crumpled balls. However, the irregular, jagged curvature of the crumpled phase is entirely extrinsic: a function of its embedding in three-dimensional space. The intrinsic, ordered, taxicab geometry of the membrane itself is unchanged through the crumpling transition.

In contrast, the phase transition we find at low temperature in the walker model changes the *intrinsic* metric of the graph from a crumpled, non-Euclidean 'Brownian map' (13) into smooth, Euclidean space. It is unclear, however, whether this Euclidean phase occurs at all temperatures for sufficiently large graphs, or only below a finite transition temperature. A renormalization group analysis of the model may shed light on this question.

Walker model. The phase transition which creates continuum geometry is driven by a statistical walker process. The motivation for this comes from the naïve curvature model, which minimizes the sum of the squares of the local discrete curvature κ, but disappointingly gives rise to a 'Medusa' phase (Figure 4b). This pathological behavior is consistent with previous investigations of triangulations, which lead to branched polymer phases and other exotic geometries rather than smooth, homogenous space (21, 29). The pathologies are due to concentrations of discrete curvature in confined regions, or large, local curvature fluctuations. Our walker process – which solves a discrete version of Poisson's equation, with the charge being the curvature κ – ultimately acts to diffuse these concentrations over large length scales.

A background for simulations. A practical application of our Euclidean graphs is as a background for simulations. Lattices, such as the square grid, are intrinsically anisotropic, so special care is often needed when designing simulations to run on them. The rotational symmetry of our graphs makes them suitable spaces on which to run simulations, such as lattice gas cellular automata (30).

Higher dimensions. We have built discrete space that behaves like two-dimensional Euclidean space at large lengths. Can the same be done for higher dimensions? While more computationally intensive, we believe our walker model generalizes to three dimensions and beyond. In three dimensions, the key step is extending the Steinitz moves in Figure 3 to add and subtract tetrahedra, rather than triangles, as nodes divide and fuse. Whether the resulting graph will be Euclidean is, however, unknown. Our tests for geodesic confinement and the applicability of Pythagoras' theorem are benchmarks for this and any other discrete models attempting to capture Euclidean geometry at large lengths.

We conjecture that the absence of geodesic confinement carries over to higher dimensional lattices, as it clearly does for the three-dimensional regular grid. Unfortunately, the proof does not readily follow from our theorem in two dimensions, which relies on planarity, since all three-dimensional lattices are non-planar. Figure 2c gives an indication of the subtlety. It shows a non-planar two-dimensional lattice that does not satisfy geodesic composition, a key step in our proof (see Methods).

Other metrics. We have shown how to grow graphs with a Euclidean metric, that is, to satisfy Pythagoras' theorem, $d^2 = x^2 + y^2$ for the distance d and orthogonal directions x and y. What about other metrics? The most sought-after of course is the Minkowski metric from special relativity, the two-dimensional analog of which is $d^2 = (ct)^2 - x^2$, where t is a time direction and c the speed of light. How to represent this as a graph is an open question, because nodes must be intricately connected at large coordinate displacements. Taking an approach similar to causal set theory (3, 4), but with neighbours separated by unit proper time, would suggest that the degree of each node diverges with the logarithm of the volume of space-time (or worse, as a power, for higher dimensions). Furthermore, unlike Euclidean space, where the square grid graph at least models a 4-fold rotational symmetry, it is not possible to construct a lattice graph which is symmetric under even a discrete version of the Lorentz transformation. Thus, it remains to be seen whether some variant of the walker process can be defined to probe and engender the fabric of space-time.

ACKNOWLEDGMENTS. The authors thank Prof. Yang-Hui He and Dr Ilia Teimouri for useful discussions.

1. Hagar A (2014) *Discrete or continuous? The quest for fundamental length in modern physics.* (Cambridge University Press, Cambridge, UK).
2. Weyl H (1949) *Philosophy of mathematics and the natural sciences* (Princeton University Press, Princeton, US), p43.
3. Bombelli L, Lee J, Meyer D, Sorkin RD (1987) Space-time as a causal set. *Phys. Rev. Lett.* 59:521.
4. Benincasa DMT, Dowker F (2010) Scalar curvature of a causal set. *Phys. Rev. Lett.* 104:181301.
5. Hamma A, Markopoulou F, Lloyd S, Caravelli F, Severini S, Markström K (2010) Quantum Bose-Hubbard model with an evolving graph as a toy model for emergent spacetime. *Phys. Rev. D* 81:104032
6. Regge T (1961) General relativity without coordinates. *Nuovo Cimento* 19:558.
7. Regge T, Williams RM (2000) Discrete structures in gravity *J. Math. Phys* 41:3964.
8. Ambjørn J, Jurkiewicz J, Loll R (2005) Spectral dimension of the universe. *Phys. Rev. Lett.* 95:171301.
9. Ambjørn J, Jurkiewicz J, Loll R (2004) Emergence of a 4D world from causal quantum gravity. *Phys. Rev. Lett.* 93:131301.
10. Horava P (2009) Spectral dimension of the universe in quantum gravity at a Lifshitz point. *Phys. Rev. Lett.* 102:161301.
11. Conrady F (2011) Space as a low-temperature regime of graphs *J. Stat. Phys.* 142:898.
12. Chen S, Plotkin S (2013) Statistical mechanics of graph models and their implications for emergent spacetime manifolds. *Phys. Rev. D* 87:084011.
13. le Gall JF (2014) Random geometry on the sphere. *Proc. Int. Congr. Math. Seoul* 1:421.
14. Krause EF (1975) *Taxicab geometry, an adventure in non-Euclidean geometry* (Addison-Wesley).
15. Erdös P, Rado R (1956) A partition calculus in set theory. *Bull. Am. Math. Soc.* 62:427.
16. Lutz FH (2008) Enumeration and Random Realization of Triangulated Surfaces. In: Bobenko AI, Sullivan JM, Schröder P, Ziegler GM (eds) *Discrete Differential Geometry*. Oberwolfach Seminars, vol 38. (Birkhäuser Basel).
17. Steinitz E, Rademacher H (1934) *Vorlesungen über die Theorie der Polyeder* (Springer).
18. Euler L (1752-3) Elementa doctrinæ solidorum. *Novi Comm. Acad. Sci. Imp. Petropol.* 4:109.
19. Bonnet O (1848) Mémoire sur la théorie générale des surfaces. *J. École Polytechnique* 19:1.
20. Metropolis N, Rosenbluth AW, Rosenbluth MN, Teller AH, Teller E (1953) Equations of state calculations by fast computing machines. *J. Chem. Phys.* 21:1087.
21. Aste T, Sherrington D (1999) Glass transition in self-organizing cellular patterns. *J. Phys. A: Mathematical and General* 32:7049.
22. Krapivsky PL, Redner S, Leyvraz F (2000) Connectivity of growing random networks. *Phys. Rev. Lett.* 85:4629.
23. Saramäki J, Kaski K (2004) Scale-free networks generated by random walkers. *Physica A* 341:80.
24. Caravelli F, Hamma A, Di Ventra M (2015) Scale-free networks as an epiphenomenon of memory. *EPL* 109:28006.
25. Wilson KG (1974) Confinement of quarks. *Phys. Rev. D* 10:2445.
26. Hardy GH, Wright EM (2008) *An introductin to the theory of numbers* (Oxford University Press, Oxford, UK).
27. Burton WK, Cabrera N, Frank FC (1951) The growth of crystals and the equilibrium structure of their surfaces. *Proc. R. Soc. Lond. A* 243:299.
28. Bowick MJ, Travesset A (2001) The statistical mechanics of membranes. *Phys. Reports* 344:255.
29. Gurau R, Ryan J (2014) Melons are branched polymers. *Annales Henri Poincaré* 15:2085.
30. Frisch U, Hasslacher B, Pomeau Y (1986) Lattice-gas automata for the Navier-Stokes equation. *Phys. Rev. Lett.* 56:1505.